Symbiosis

www.symbiosisonline.org
www.symbiosisonlinepublishing.com

Research Article | International Journal of Plant studies | Open Access

Plant Cell Wall Dynamics are Regulated by Intercellular Sugar Trafficking

M. Best[1,3], M.J. Schueller[2] and R.A. Ferrieri[2*]

[1]Fachbereich Chemie, Johannes Gutenberg Universität, 55099 Mainz, Germany

[2]University of Missouri, Missouri Research Reactor Center, Department of Chemistry, Columbia, MO, 65211

[3]Present address: Miltenyi Biotech GmbH, Robert-Koch-Str. 1, 17166, Teterow, Germany

Received: June 27, 2018; Accepted: July 6, 2018; Published: July 10, 2018

***Corresponding author:** Richard A. Ferrieri, [2]University of Missouri, Missouri Research Reactor Center, Department of Chemistry, Columbia, MO, 65211; E-mail: FerrieriR@missouri.edu*

Abstract

Cellulose biosynthesis in plant cell walls is continually modified to accommodate developmental stages of the plant and to respond to environmental changes. Here we used radioactive isotopes of ^{11}C ($t_{1/2}$ 20 m), administered to leaves as $^{11}CO_2$, and ^{18}F ($t_{1/2}$ 110 m), administered to roots as the glucose analogue, 2-deoxy-2-[^{18}F] fluoro-D-glucose (^{18}FDG), and developmental leaf aging in Nicotiana tabacum to explore the different contributions of intracellular (^{11}C) sugar versus the exchange of intercellular (^{18}F) sugar. Leaf cellulose content decreased with leaf age, and was correlated with a decreasing influx of ^{18}F tracer. However, the incorporation of intracellular ^{11}C sugar into cellulose was unchanged with leaf age, suggesting that the rate limiting step in controlling cellulose biosynthesis was the intercellular exchange of sugar. This hypothesis was tested using known inhibitors of cellulose biosynthesis. Isoxaben, a pre-emergence herbicide and methyl jasmonate, a plant defense hormone, were topically applied to same aged source leaves prior to tracer administration. Treatments exerted opposite effects on sugar transport, as well as opposite effects on ^{11}C and ^{18}F tracer flux into cellulose. These combined results support the model where cellulose biosynthesis was tightly coupled to intercellular sugar trafficking and not to the state of the metabolic machinery.

Keywords: Intercellular sugar trafficking; cellulose synthesis; developmental aging; carbon-11; ^{18}FDG;

Introduction

Plant cell walls are complex macromolecular structures that surround cells and are compositionally rich in polysaccharides, proteins, aromatic compounds and aliphatic compounds. They are highly dynamic compartments, differentiated by cell type and developmental stage, and serve a multitude of important aspects to plant survivability under various environmental conditions [1, 2].

Growing or expanding cells are typically surrounded by a primary wall comprised largely of polysaccharide macromolecules which contribute to the structural integrity of the cell and to cell adhesion. This structure provides an important conduit for solute transfer including growth resources and key signal molecules that help maintain cellular function [3].

In many cells, this wall can be thickened and further strengthened by the addition of a secondary wall containing lignin, or polyaromatic macromolecules that help maintain cellular water conductance. As plant cells continue to grow, becoming more specialized in function and differentiated by the tissue type, the walls that encase them often can possess a vast array of compositional differences that help serve the diverse cellular functions across the plant.

Plants are sessile organisms, and as such have evolved with the capacity to be highly plastic in their responses to growth conditions imposed by a changing environment. This unique feature empowers them with the ability not only to survive harsh conditions, but also to survive predation by herbivores and attack by pathogens. Their ability to respond in this capacity requires that the cell wall structure, and its composition, be continually modified providing physical barriers as a mechanism to ward off attack by predators. For example, strategically situated parenchyma cells will rapidly develop invaginations or reinforcements of their cell wall as a consequence of plant defense [4]. Jasmonic acid (JA) and it's methyl ester are key hormones that trigger this response by stimulating re-programming of key biochemical pathways providing essential biosynthetic precursors for lignin as a physical barrier [5,6]. In parallel, JAs also mediate reduced biosynthesis of cellulose, the most abundant polysaccharide macromolecular component of cell walls, and likely the most nutritious to feeding herbivores [7, 8].

The highly dynamic nature of cellulose biosynthesis attests to the complexity of the underpinnings that regulate cell wall construction. To this day, that regulation is still not entirely understood, especially in the context of changing cellular functions that coincide with normal plant growth and development [2, 3,9,10 and 11]. To properly generate or modify the cell wall, proteins involved in the process, including cellulose

synthesis, glucan synthesis and pectin methyl esterase, are transported intracellular via membrane trafficking to the plasma membrane, or the extracellular space [12,13]. It is presumed that such processes must be tightly regulated [14]. Recent studies even go as far as to suggest that the diversification of membrane trafficking is what contributes to cell wall differentiation across all plant cell types [15]. Even so, there remain many open questions concerning the molecular mechanisms that underlie these transport processes. For example, some proteins at the plasma membrane may become endocytosed into the cytoplasm in response to feedback signals associated with extracellular conditions [16].

Unfortunately, very little attention has been given to understanding the dynamics underpinning the exchange of the simple sugar building blocks that are important to cell wall construction and/or modification. Herein, we report on the use of a short-lived radiocarbon isotope, carbon-11 ($t_{½}$ 20.4 min), administered to intact leaves in Nicotiana tabacum as $^{11}CO_2$ to explore the effect of leaf age on the intracellular partitioning of "new carbon" into cell wall cellulose [17]. We also report on the use of the fluorine-18 ($t_{½}$ 110 min) radioisotope, administered to plants as 2-[^{18}F]fluoro-2-deoxy-D-glucose (^{18}FDG), a radioactive glucose surrogate, to examine the role of intercellular sugar trafficking in cellulose biosynthesis using developmental leaf aging as a model [18]. Over the years, fluorine- 18 has been extremely useful for radio-labeling molecules of interest for use in animal and human research, but in recent years this isotope has found its way into plant science with the radio synthesis of ^{18}F-labeled sucrose analogues to study sugar transport [19, 20]. Additionally, ^{18}FDG has also been shown to actively transport in plant vasculature [21-26] and utilized in secondary metabolism of essential defense compounds [27]. Here, we showed evidence that plants will metabolically assimilate ^{18}FDG into cell wall cellulose and the tracer can be used as a marker for quantifying extracellular glucose flux into cellulose.

Materials and Methods

Plant Growth: Tobacco plants (Nicotiana tabacum L. cv Samsun) were grown from seeds in commercial potting mix with a slow-release fertilizer (Osmocote; Scotts Company, Marysville, OH, USA) in commercial growth chambers (Conviron, Inc., Winnipeg, Canada) at 24°C with a 16/8 h photoperiod at 350 µmol m^{-2} s^{-1}. At 3 weeks into their growth cycle, seedlings were transferred to aerated hydroponics stations (8 plants per station). The nutrient status in the hydroponics solution was maintained using commercial a Hoagland modified basal salt mixture (PhytoTechnology Laboratories, Shawnee Mission, KS, USA) prepared by dissolving 4.9 g of the salt mix in 3 L of de-ionized water and buffering with 1.66 g MES hydrate. The pH of the solution was adjusted to 6.5 by adding 1N potassium hydroxide solution. Hydroponics solutions were changed on a 5-d cycle. Plants were used for experiments when they had seven fully expanded leaves.

Treatments: All chemicals used in these studies were obtained from Sigma Aldrich (St. Louis, MO, USA) and were used without any further purification. Isoxaben (ISX), N-(3'[1-ethyl-l-methylpropyl]-5-isoxazolyl)-2,6-dimethoxybenzamide is a pre-emergence, broad leaf herbicide used primarily on small grains, turf grasses and ornamental plants [28].

This herbicide is extremely active, with IC50 values in the nanomolar range [29]. Isoxaben treatment has been shown to selectively inhibit 14C-glucose incorporation into the acid insoluble cellulosic cell wall fraction [30,31] and so has become a powerful tool enabling the chemical inhibition of cellulose biosynthesis in vivo.

Isoxaben interferes with rosette formation, and by blocking the demonization of CesA polypeptides 130 it inhibits cellulose biosynthesis [32]. Jasmonic acid (JA), including its methyl ester (MeJA), is ubiquitous in all higher plants filling numerous roles in plant growth and development [33] and especially plant defense hormones eliciting rapid reprogramming of plant metabolism when applied topically to tissues [5,34]. Like ISX, MeJA will also inhibit cellulose biosynthesis in vivo. In all tracer flux measurements involving measuring radio labeled cellulose, we applied either a 5 nm solution of ISX or a 5 µM solution of MeJA as topical treatments to upper intact leaf surfaces. Differences in treatment concentrations were based on perceived substrate biological activities. Treatments were applied to a small single layer section of Kim Wipe™ for 1 hr prior to tracer administration (i.e. $^{11}CO_2$ to leaves or ^{18}FDG to roots). In special studies designed to assess the effect of treatment dose on ^{11}C-photoassimilate transport, we administered treatments through the cut petiole of an excised leaf. The amount of treatment taken up by the leaf tissue was quantified by measuring the volume of solution assimilated over time. Treatment solutions were significantly reduced for this experimental protocol because a significant volume of solution was always assimilated by the cut leaf over a 1hr time course.

$^{11}CO_2$ Production and Leaf Administration: $^{11}CO_2$ was produced via the $^{14}N(p, \alpha)^{11}C$ nuclear transformation from a 20 ml target filled with high-purity nitrogen gas (400 ml @ STP) using 18MeV protons from the TR-19 (Ebco Industries Ltd, Richmond, BC, Canada) cyclotron at BNL, and captured on a molecular sieve (4Å). The $^{11}CO_2$ that was trapped on the molecular sieve was desorbed and quickly released into an air stream at 200 ml/min as a discrete pulse for labeling a leaf affixed within a 5 x 10 cm lighted (350 µmol m^{-2} s^{-1}) leaf cell at 21°C to ensure a steady level of fixation [35, 36]. For mature source leaves, only a portion of the leaf was affixed within the cell. The leaf was positioned in the cell so as to capture part of the outside leaf edge. This configuration allowed efficient air/tracer flow around the upper side of the leaf as well as the underside. The load leaf tissue was exposed to $^{11}CO_2$ tracer for 1 minute as a transient pulse in the air stream, and then was chased with clean air for the duration of the exposure. A PIN diode radiation detector (Carroll Ramsey Associates, Inc, Berkeley, CA, USA) affixed to the bottom of the leaf cell enabled continuous measurement of radioactivity levels within the cell during the pulse.

^{18}FDG Synthesis and Root Administration: Fluorine-18 as fluoride anion (^{18}F-) was produced using an 18 MeV proton beam on the TR-19 cyclotron (Ebco Industries Ltd, Richmond, BC, Canada). This beam was focused onto an oxygen-18 enriched water target causing the ^{18}O (p, n) ^{18}F nuclear reaction to occur. After irradiation, ^{18}F-fluoride was collected on a QMA sep-pak (Waters Accell Plus QMA) located at the target station, then extracted and transferred under pressure to the radiochemistry laboratory using a dilute solution of acetonitrile and potassium bicarbonate (0.1 N). The contents of the transfer were received into a FDG-Plus™ Automated Radiochemistry Module (Bioscan, Inc., Washington, DC, USA) where the ^{18}F-fluoride was dried under vacuum with Kryptofix 2.2.2. ^{18}F-Fluoride was then reacted with mannose trifoliate (1, 3, 4, 6-tetra-O-acetyl-2-O-trifluoromethane sulfonyl-β-D-mannopyrannose). Reaction by nucleo philic displacement with the trifoliate starting material yielded an intermediate radio labeled product in high yield that could be hydrolyzed easily in base and at room temperature to yield 2-deoxy-2- [^{18}F]fluoro-D-glucose (^{18}FDG). The reaction mixture was processed through a C18 Sep-Pak cartridge to remove the phase-transfer catalyst, Kryptofix 2.2.2. The final product was formulated in approximately 1 ml of de-ionized water yielding approximately 5 mCi per dose of purified product at end-of-synthesis. Doses were measured using a CRC-12 Dose Calibrator (Capintec, Inc., Ramsey, NJ, USA).

^{18}FDG was administered directly to the hydroponics solution of study plants. In staging these studies, individual plants were removed from their larger hydroponics growth chambers and transferred to individual 50 ml beakers filled with 30 ml de-ionized water. Forced air from an aquarium air pump maintained proper solution aeration and provided good mixing of the tracer. Studies leveraging ^{18}F-fluoride as a water flow tracer were conducted in the same manner as the ^{18}FDG studies. For ^{18}F-fluoride uptake studies, the dried tracer was reconstituted in 1 mL of de-ionized.

Leaf Autoradiography: Counting down from the apex, leaf-2 (a nearly fully expanded source leaf) was subjected to topical treatments while still attached to the plant. MeJA or ISX treatments were applied on half of the leaf's upper surface, as described above. 2.5 hour following ^{18}F-fluoride or ^{18}FDG tracer administration to the roots, leaf-2 was excised and imaged for quantifying either ^{18}F-fluoride or ^{18}FDG uptake and distribution using autoradiography (Typhoon 7000: GE Healthcare, Piscataway, NJ, USA). Differences in the radioactivity levels between the 190 treated and untreated halves were determined using Image Quant TL 7.0 software (GE Healthcare Bio-Sciences AB, Uppsala, Sweden) where 1 cm diameter circular regions-of interest (ROI) we retraced onto both sides of the leaf's midrib (placed equidistant from that reference point), and the amount of radioactivity within each ROI was determined from the image intensity. No correction was made for tissue attenuation of radioactivity in the acquired images since it was assumed that each leaf half was identical in nature and thickness to the other.

Autoradiography was also used in ^{11}C tracer studies. In these studies, leaf-2 was detached from the plant to enable treatments to be administered via the cut petiole (see Treatment section for details). Gaseous $^{11}CO_2$ tracer was administered to the detached leaf in much the same way as in the intact leaf studies and autoradiography was used to quantify ^{11}C-photoassimilate transport(after $^{11}CO_2$ fixation) as a function of treatment type and treatment dose. Imaging was performed 30 min after $^{11}CO_2$ fixation to avoid ^{11}C-photoassimilate transport beyond the "field-of-view" resulting in exudation of tracer out through the petiole cut. Using the same Image Quant software, ROIs were traced around the $^{11}CO_2$ fixation site, as well as the remaining leaf tissue including petiole outside that site which contained radioactivity. The amount of activity found outside of the fixation site was correlated to transported ^{11}C-photoassimilate.

Magnetic Resonance Imaging: A single intact leaf imaging experiment was conducted using BNL's 4-Tesla MRI scanner as a way to verify the utility of the ^{18}F-fluoride tracer as a water flow agent in plants. Past studies [37, 38 and 39] have attested to the fact that this tracer can be used as a proxy for tracing the dynamics of water transport in plants. Even so, we designed our own test. In a single experiment we compared leaf autoradiography (Figure. 1) of ^{18}F-fluoride distribution in a 'masked' leaf study with that of a proton MRI of the same 'masked' leaf. Half of the leaf was masked using an opaque cardboard cover. The other half was illuminated using an LED illuminated fiber optic wand that allowed us to transmit light to the leaf surface while the plant was positioned within the magnet's bore.

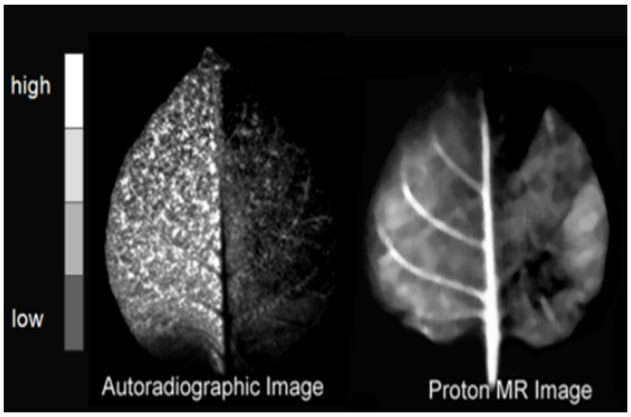

Figure 1: Left-side panel shows the radioactivity distribution from a phosphorplate image of a tobacco leaf after root exposure to ^{18}F-fluoride as a water mimic. The right side of the leaf was shaded as a treatment for changing leaf water conductance. The right-side panel shows a proton magnetic resonance image of a tobacco leaf using the BNL 4T MR. Here too, the right side of the leaf was shaded to test for changes in leaf water conductance. A gray scale bar was used to reflect levels of high radioactivity or high proton MR signal.

The BNL 4-Tesla MRI scanner was driven by a Varian INOVA console with a shielded whole-boy SONATA-Siemens gradient set (using three K2217 Siemens Cascade Gradient Power Amplifiers with 2000 V and 500 A) to produce gradient pulses with 44 mT/m peak amplitude at 0.25 m sec maximum rise time. A multiple-spin-echo series of pulses was applied as a train of 180o rf pulses giving a series of echoes with a single phase encoding gradient [40]. By varying the phase encoding gradient, a spin-echo image

can be obtained that can be translated into a planar T2 mapping of tissue water content.

Whole-Plant ^{18}FDG Translocation: The movement of ^{18}FDG from roots up into the shoots and leaves of the plant was monitored using two sodium iodide scintillation detectors (Ortec, Oak Ridge, TN, USA) that were positioned facing perpendicular to the apex area and to leaf-2. Each detector was well-shielded using small tantalum blocks to ensure minimal detector crosstalk.

Detectors were cross-calibrated against a NIST traceable point source of radioactivity prior to each experiment. Each detector was set to report radioactivity levels on 1 min time intervals. The temporal allocation patterns of radiotracer translocation to the apex region and to leaf-2 were based on the amount of tracer assimilated by the plant over the time course of the experiment, and reported as fractional total activities. The amount of tracer assimilated by the plant was determined by measuring the level of radioactivity in the beaker (after the plant was removed at the end of the experiment) and comparing that value to the original dose of administered. All calculations were performed using decay corrected values to account for ^{18}F radioisotope decay over time.

^{18}FDG-6-Phosphate Metabolite Analyses: Approximately 100 mg of leaf-2 tissue was extracted 2.5 hr after ^{18}FDG was administered through the roots of the plant. Extraction was carried out in 4x w/v of methanol, briefly vortexes (VWR analog vortex mixer; Sigma-Aldrich Corp. St. Louis, MO, USA) and then sonicated (Branson Bransonic 32; Sigma-Aldrich Corp. St. Louis, MO, USA) in an iced water bath for 10 min. The tubes were centrifuged (Eppendorf Centrifuge 5424) for 2 min at 15,000 rpm and the supernatant was filtered through 0.2 µm Acrodiscs (Gelman Sciences, Ann Arbor, MI, USA). An aliquot of the extract was analyzed by radio-TLC [41] using silica gel–coated plastic sheets (Polygram SIL G/UV254; Macherey-Nagel) and acetonitrile/tetrabutylammonium hydroxide, 9.5 mmol/L, 8:2 (v/v), as eluent. The formation of ^{18}FDG-6-P was confirmed by co-spotting the TLC plate with 245 nonradioactive ^{19}FDG-6-P (Sigma-Aldrich, St. Louis, MO USA).

Doses of pure ^{18}FDG-6-P were prepared using in vitro enzyme chemistry and applied to leaf tissue to test for ^{18}FDG-6-P mobility. To generate these doses, 5 mCi of ^{18}FDG was added to 1 ml NaH_2PO_4 buffer solution (70 mmol/L) that contained 10 mg (250–400 units) of hexokinase type IV from bakers' yeast (EC 2.7.1.1; Sigma-Aldrich, St. Louis, MO USA), 2 mg (3.6 µmol) of adenosine triphosphate (Sigma-Aldrich, St. Louis, MO USA) and 1 mg (5 µmol) $MgCl_2 \cdot 6H_2O$ (Sigma-Aldrich, St. Louis, MO USA) and was pH adjusted to 7.4. The solution was stirred at room temperature (30°C) for 60 min and samples taken for radio-TLC analysis of product purity (Figure 2) ^{18}FDG-6-P transport assays were carried out by applying tracer to an abraded leaf surface and measuring the extent of transport over 1 hr using autoradiography.

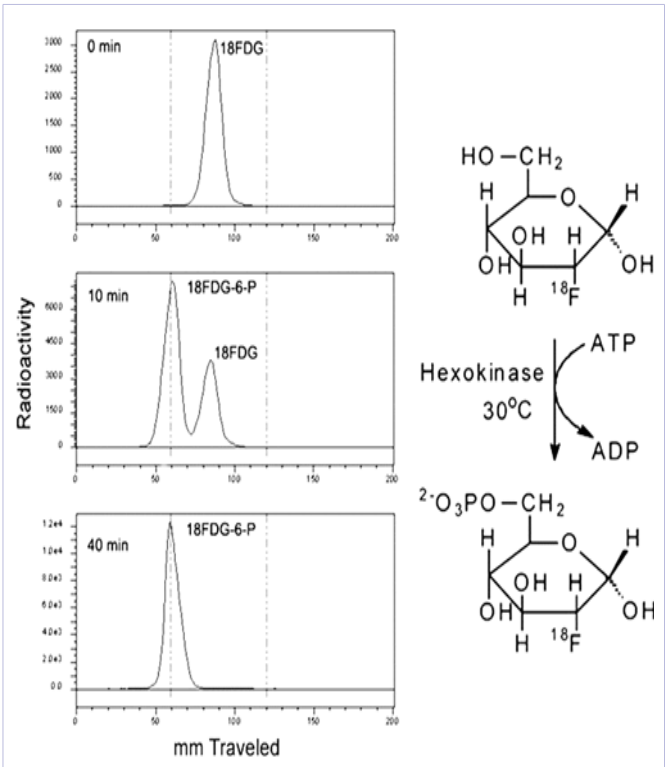

Figure 2: This figure shows the time course for *in vitro* enzymatic conversion of ^{18}FDG to ^{18}FDG-6-P. Radio thin layer chromatography was used to separate the two substrates. The same TLC method was used to analyze leaf tissue extract for extent of ^{18}FDG phosphorylation.

Measurement of Leaf [^{11}C] Cellulose and [^{18}F] Cellulose

One hour after $^{11}CO_2$ tracer was administered to either the young apex leaves or the older source (leaves 2, 4 or 6), the respective leaf was excised from the plant at the petiole. The tissue area that was captured in the leaf cell during tracer exposure was then cut away from the remaining leaf tissue, weighed, and then flash frozen in liquid nitrogen. Using a mortar and pestle, the tissue was powdered in liquid nitrogen, and extracted using published procedures [17, 42-45]. In the first step the tissue was refluxed in 6 ml of aq MeOH (50% v/v) for 10 min at 90°C. The extract was separated by pipette, and the remaining tissue was washed twice using 6 ml of demonized water. The washings were combined with the aqueous alcohol fraction prior to counting the ^{11}C. This fraction removed small soluble compounds including radio labeled monosaccharides and disaccharides and amino acids that were subjected to separate radio-HPLC analyses discussed below. The remaining tissue (considered cell-wall components) was subjected to an extraction using 6 ml of dilute 1 N Naoh for 10 min at 95°C. This step separated callose (1,3-β-glucans), as well as pectin's (branched chain 1,4-β-glucans) from the remaining cell wall polymers. The extract was again separated by pipette, and the remaining tissue washed twice using 6 ml of de-ionized water. The washings were combined with the base portion prior to counting the ^{11}C. The remaining tissue was then subjected to acid digestion using a 3:1 mixture of dilute 1 N nitric acid: acetic

acid for 30 min at 100°C enabling hemicelluloses to be solubilized, leaving behind cellulose as the undigested portion. The contents were cooled to ambient temperature and filtered onto 2-cm disks of pre-weighed glass microfiber filters (GF/A: 2.5 cm diameter; What man, Maid stone, UK). The collected tissue was washed 3-times during this filtration step using de-ionized water. Samples were immediately counted using a static NaI gamma radiation detector, decay-corrected back to a common zero time and fraction-corrected to allow correlation to total ^{11}C-activity fixed within the tissue. Once counted, filtered samples were dried under a heat lamp and reweighed to determine 280 the amount of cellulosic biomass.

This same cellulose analysis protocol was used to measure ^{18}F-cellulose derived from^{18}FDG, and in one study application from ^{18}FDG-6P. Unlike the ^{11}C-tracer studies, leaf tissue samples were harvested for ^{18}F-cellulose analysis 2.5 hr after ^{18}FDG tracer was administered to the roots. We tried to target the same region of leaf tissue and mass as in the ^{11}C-tracer studies. A longer time period was used in the ^{18}F-tracer studies than in the ^{11}C-tracer studies to allow sufficient time for initial uptake and transport of ^{18}F-tracer to the aerial portions of the plant. At the end of the cellulose assay, the acid indigestible portion was dried and further deconstructed using the phenol–sulfuric acid assay [46]. This method involved refluxing the material in a 1:10 solution of phenol (5%) and concentrated sulfuric acid at 100oC until all of the solid material was digested. Aliquots of this extract were neutralized and analyzed by radio HPLC for recovered ^{18}FDG.

Measurement of Leaf Water Potential: In a separate set of measurements, leaf water potentials (Ψ) were determined for a set of different aged leaves by using a Scholander pressure bomb (model 3005, Soil moisture Equipment Corp., Santa Barbara, USA).

Statistical Analysis: Data was subjected to the Student t-test for unpaired samples assuming an unequal variance. Statistical significance levels were assigned to the following rating scale (*, P <. 05; **, P <. 01; ***, P <. 001).

Results

Characterization of ^{18}FDG Uptake and Translocation in Plants: ^{18}FDG was taken up by intact plant roots and transported to the aerial portions of the plant via the xylem. This process was driven by water flow regulated by the plant's transpiration stream. On arrival into mature leaves, ^{18}FDG can be phosphorylated or utilized in cell-wall construction. In either case the ^{18}F-tracer becomes immobilized. Additionally, ^{18}FDG delivered into mesophyll cells could be converted to^{18}F-sucrose or some other mobile metabolite that is reloaded into the phloem and transported across long-distances to distal sink tissues such as young developing leaves and roots. Results in (Figure 1) reflect this dynamic exchange over a 4 hour time period. We observed that mature leaf-2 radioactivity, presented as a ratio of tissue radioactivity divided by the total plant radioactivity, increased during the early stages of ^{18}FDG incubation, and then decreased during the later time points.

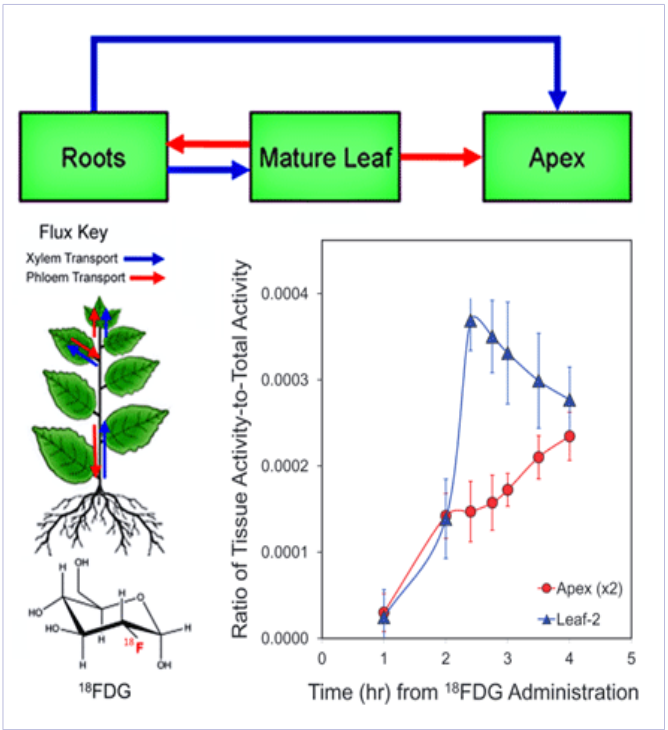

Figure 3: ^{18}FDG is taken up by roots and transported to aerial portions of the plant via the xylem and driven by water transpiration. Once in source leaves, ^{18}F-tracer derived from xylem unloading of ^{18}FDG can be loaded into the phloem and transported to sink tissues (e.g. young developing leaves in the apex and the roots). Data reflects mean values ± SE on at least N=3 plants.

All data presented in Fig. 3 was corrected for radioactive decay so this trend reflected phloem re-loading and long-distance transport of ^{18}F-tracer. In concert with this behavior, radioactivity in the plant's apex was seen to pass through an inflection point that was slightly delayed in time from the maximum activity time point in leaf-2. This too is a reflection of phloem loading and long-distance transport of ^{18}F-tracer from the source leaf to this sink.

Treatments using ISX and MeJA Impact ^{18}F-Tracer Mobility: Chemical inhibitors for cell-wall cellulose, isoxaben (ISX) and methyl jasmonate (MeJA) were tested for their effects on ^{18}F-tracer mobility derived from ^{18}FDG. Treatments were applied to half of leaf-2, and autoradiography was used to quantify effects of treatment on phloem loading of the ^{18}F-tracer (Figure 4). Data was presented as a ratio of the treated tissue activity divided by the untreated tissue activity (T/U) that was measured across the two halves of same leaves. Control data was derived from application of mock treatments using deionized water. Results from these studies were summarized in (Table 1). This table also contained data on the effect of treatment on leaf water flow where ^{18}F-fluoride was used as a water tracer. We felt that it was important to access treatment effects on water flow as this dynamic had a strong bearing on xylem unloading of ^{18}FDG into leaf-2. Furthermore, Table 1 also contained data on the effect of treatment on ^{18}FDG phosphorylation as this process would impact ^{18}F-tracer mobility in phloem loading, as well as remove ^{18}F-tracer from metabolically active sugar pools used in cellulose

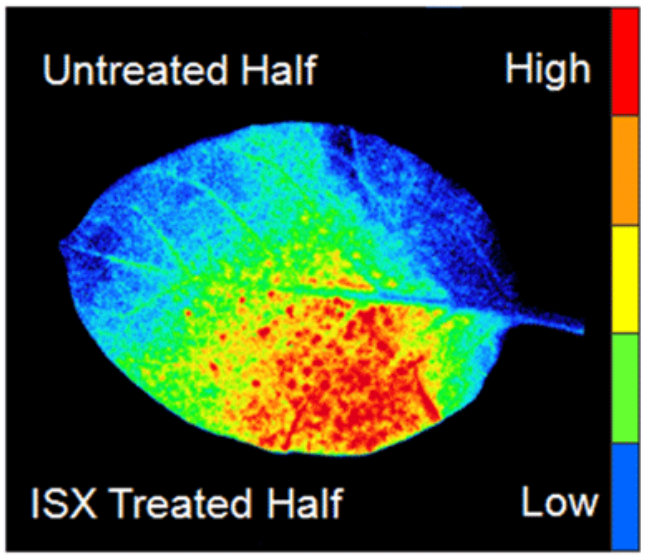

Figure 4: Phosphor plate image of a tobacco leaf-2 removed from a plant after root exposure to ^{18}FDG. Half of the leaf was treated with either ISX or MeJA while the other half was untreated. In the image shown, an ISX treatment was used. A graded color scale was applied to reflect differing levels of radioactivity (red, high; blue, low).

biosynthesis. Our application of ^{18}FDG-6P to leaf tissue showed no evidence of physical transport, nor evidence of chemical assimilation of ^{18}F-tracer into cellulose (data not shown). Taken together, we were able to correct ^{18}F-tracer mobility data for changes in leaf water conductance and for changes in ^{18}FDG phosphorylation imposed by the chemical treatment (see bottom row in Table 1). In summary, ISX treatment had no significant effect on ^{18}FDG delivery to leaf-2 by the xylem nor did it have a significant effect on ^{18}FDG phosphorylation in that tissue, but it did significantly reduce ^{18}F-tracer loading into the phloem, as reflected by the significantly higher T/U value relative to controls, 1.820 ± 0.116 versus 0.949 ± 0.123, respectively (P=0.0009). In contrast, MeJA treatment significantly reduced ^{18}FDG delivery to leaf-2 by the xylem, it slightly increased

^{18}FDG phosphorylation and it slightly increased ^{18}F-tracer loading into the phloem as reflected by the lower T/U value relative to controls, 0.546 ± 0.373 versus 0.949 ± 0.123, respectively (P=0.0520).

Treatments using ISX and MeJA Impact ^{11}C-Photoassimilate Transport.

Similarly, ISX and MeJA treatments were tested for their impact on ^{11}C-photoassimilate transport in leaf-2. In these studies

Table 1: Leaf-2 Radioactivity Profile

Metric	Treatment	Avg. Ratio (T/U)[a]	Sample Size	Std. Dev.	Std. Error	P-Value
^{18}F-Fluoride Distribution	Control	1.036	5	0.164	0.073	--
	ISX	0.858	4	0.185	0.092	0.1685
	MeJA	0.497	4	0.219	0.109	0.0038
^{18}FDG Distribution	Control	0.995	3	0.096	0.055	--
	ISX	1.993	6	0.266	0.109	0.0005
	MeJA	0.396	5	0.164	0.074	0.0013
^{18}FDG Metabolism[b]	Control	1.013	3	0.12	0.069	--
	ISX	1.29	3	0.211	0.122	0.1195
	MeJA	1.45	3	0.257	0.148	0.0559
Adjusted ^{18}FDG Distribution[c]	Control	0.949	--	--	0.123	--
	ISX	1.82	--	--	0.116	0.0009
	MeJA	0.546	--	--	0.373	0.052

1. Ratio of decay corrected radioactivity between treated (T) and untreated (U) halves of leaf-2, 4 hr after administration of the tracer to plant roots.
2. ^{18}FDG metabolism was based on the extent of its conversion to the non-transportable 6-phosphorylated sugar.
3. This calculated ^{18}FDG distribution makes adjustments for treatment effects on water input using ^{18}F-fluoride distribution data and adjustments for treatment effects on ^{18}FDG metabolism to its non-transportable form as 6-P-^{18}FDG once in the targeted leaf-2 tissue. Standard propagation of error was applied. Distribution values higher than unity suggest a reduction in phloem reloading.

the leaf was detached, and treatment was applied through the cut petiole (Figure 5) prior to administration of $^{11}CO_2$. As before, autoradiography was used to quantify effects of treatment on phloem loading and transport of ^{11}C-photoassimilates within the leaf.

The distance tracer traveled from the boundary of the $^{11}CO_2$ leaf cuvette over a fixed period of time was used as the metric of transport. Since treatments were applied via the cut petiole, it was also possible to quantify the dose assimilated by the study leaf during the incubation period and map transport against treatment in a dose dependent manner. Treatments were applied over 107 orders of magnitude ranging from 0.004 pmol • g fresh wt^{-1} leaf tissue to 50,000 pmol • g fresh wt^{-1}.The results in (Figure 6)were plotted on a logarithmic scale to reflect the exponential

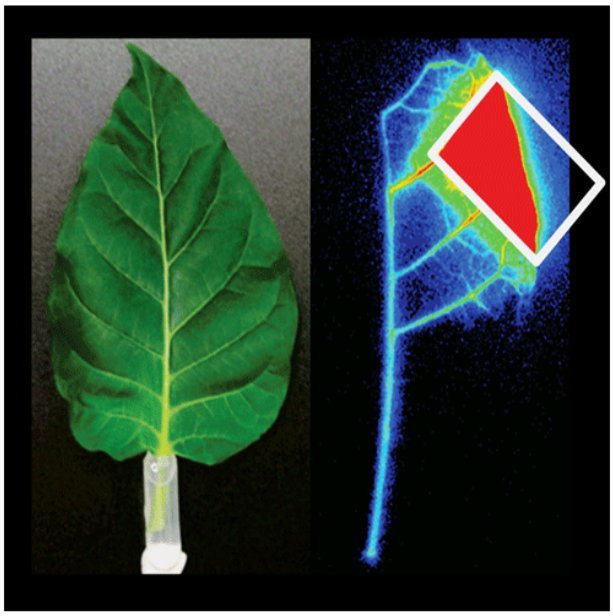

Figure 5: The left-side panel shows a photograph of the experimental setup whereby the petiole of a cut leaf was placed in a small plastic tube filled with either just deionized water, or a solution of ISX or MeJA treatment. The right-side panel shows a phosphor plate image indicating ^{11}C-photoassimilate transport after administration of $^{11}CO_2$ tracer. In the color scale, red indicates regions of high ^{11}C activity while blue indicates regions of low activity. The white box in the image shows an overlay of where the leaf cell was affixed to the leaf during tracer administration.

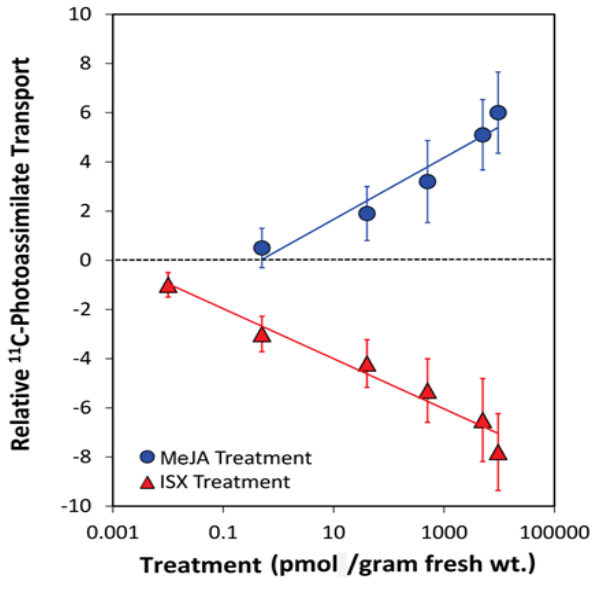

Figure 6: Plot showing change in relative ^{11}C-photoassimilate transport relative to dose of ISX and MeJA treatments assimilated by the tissue in cut leaf experiments. The dotted 'zero' line reflects the average transport of ^{11}C-photoassimilate in an untreated leaf. MeJA treatment increased ^{11}C-photoassimilate transport exponentially relative to controls. In sharp contrast, ISX decreased ^{11}C-photoassimilate transport exponentially relative to controls. Data reflect at least three replicates with standard errors.

dose dependencies of ^{11}C-photoassimilate transport to both treatments. Transport was normalized in this figure relative to control (untreated) studies which was shown as the 'zero' dotted line.

Positive deviation from this 'zero' line reflected increased ^{11}C-photoassimilate transport, whereas negative deviation from this line reflected decreased transport. Similar to the ^{18}FDG results, ISX treatment significantly decreased ^{11}C-photoassimilate transport in a dose dependent manner while MeJA significantly increased transport.

Leaf Age Impacts Tracer Flux into Cellulose

Leaves at different stages of development (apex, leaf-2, leaf-4 and leaf-6) were tested to determine whether developmental leaf age influenced the extent of intracellular sugar (^{11}C) and intercellular sugar trafficking (^{18}F) contributed to cell-wall cellulose biosynthesis. Results from these studies were presented in Table 2 along with cellulose content data that was presented as percent gram fresh weight (% gfw) of leaf tissue. Cellulose content decreased significantly from 1.024 ± 0.048 % gfw to 0.399 ± 0.124 % gfw with increasing leaf age. Leaf water potentials also increased from -0.35 ± 0.03 to -0.22 ± 0.01 MPa across the same range of leaf ages resulting from increased water content in the older leaves.

This phenomenon would inherently lower the measured values of the cellulose content with increasing leaf age when based on fresh tissue mass, but the magnitude of the observed drop in cellulose content (61%) exceeded the change in water potential (37%), so likely the measured decrease in cellulose with increasing leaf age was real. However, ^{11}C-cellulose content remained unchanged with leaf age while ^{18}F-cellulose decreased significantly from 0.083 ± 0.011 % of tissue radioactivity to 0.010 ± 0.007 % of tissue radioactivity with increasing leaf age.

Treatments using ISX and MeJA Impact Tracer Flux into Cellulose

Having placed the impact of ISX and MeJA treatments on cellular sugar transport in a proper context, we next conducted tests to see if these treatments had any impact on the flux of tracers (^{11}C vs.^{18}F) into leaf-2 cellulose. The results in Table 3 showed that ISX and MeJA treatments impacted the flux of ^{11}C-tracer into ^{11}C-cellulose, increasing it from 0.282 ± 0.019 % of leaf-2 radioactivity in controls to 0.406 ± 0.051 % with ISX treatment (P = 0.0527), and significantly decreasing it to 0.090 ± 0.026 % with MeJA treatment (P = 0.0003). These same treatments were found to have just the opposite effect on the flux of ^{18}F-tracer (as ^{18}FDG) into ^{18}F-cellulose where ISX significantly decreased the flux from 0.042 ± 0.003% of leaf-2 radioactivity in controls to 0.021 ±0.001 in treated tissues (P = 0. 0010), while MeJA significantly increased the flux to 0.055 ± 0.005 in treated tissues (P = 0.0496).

Table 2: Effect of Leaf Age on Tracer Flux into Cellulose

Leaf type	^{11}c-Cellulos[a]	std. Dev.	std. Error.	sample size	^{18}F Cellulose[b]	std. Dev.	std. Error.	sample size	cellulose content (%gfw)[c]	std. Dev.	std. Error	sample size
Apex	0.263	0.012	0.006	4	0.083	0.033	0.011	9	1.024	0.136	0.048	8
Leaf-2	0.282	0.043	0.019	5	0.042	0.01	0.003	9	0.754	0.129	0.043	9
Leaf-4	0.259	0.063	0.028	5	0.029	0.018	0.008	5	0.496	0.211	0.094	5
Leaf-6	0.279	0.091	0.053	3	0.01	0.013	0.007	3	0.399	0.215	0.124	3

a. Presented as the percentage of fluorine-18 activity within the extracted tissue.
b. Calculated by dividing the dried cellulose mass by the grams fresh weight (gfw) of tissue extracted.
c. Presented as the percentage of carbon-11 activity within the extracted tissue.

Table 3: Effect of Treatment Type on Tracer Flux into Leaf-2 Cellulose

Treatment	^{11}C Cellulose[a]	Std. Dev.	Std. Error	Sample size	P-Value	^{18}F-Cellulose[b]	Std. Dev.	Std. Error	Sample size	P-Value
Control	0.282	0.43	0.019	5	--	0.042	0.01	0.003	9	--
ISX	0.406	0.115	0.051	5	0.0527	0.021	0.006	0.001	5	0.001
MeJA	0.09	0.058	0.026	6	0.0003	0.055	0.012	0.005	6	0.0496

a. Presented as the percentage of carbon-11 activity within the extracted tissue.
b. Presented as the percentage of fluorine-18 activity within the extracted tissue.

Discussion

Over the years, most attention has been given to the transport of sucrose as it represents the major mobile form of photo synthetically assimilated carbon in higher plants [47, 48]. Sucrose synthesized in fully mature source leaves is exported via the phloem to supply non-photosynthetic organs with energy and carbon resources. Its long-distance transport requires loading of sucrose into phloem sieve elements from symplastic or apoplastic compartments [49, 50]. This is facilitated by sucrose transporters (SUT), also called sucrose carriers (SUC), which are driven by negative plant potentials. In Nicotiana tabacuum, the sucrose transporter 1 protein (SUT1) responsible for transporting sucrose over long-distances functions as a H^+/sucrose symporter [51,52].

Since the identification of the first eukaryotic monosaccharide transporter in Chlorellakessleri [53], monosaccharide transporters have also been identified in a variety of higher plants [54-57]. For example, in Arabidopsis thaliana, the AtSTP1 and AtSTP3 monosaccharide transporters display both high and low affinity for D-glucose transport, respectively, suggesting functional differences [58, 59]. Marked differences in the pattern of expression have also been noted across tissues, organs and even cell types. For example, AtSTP1 transcripts are present in leaves, stems, flowers, and roots, while AtSTP2 is expressed only in developing pollen [60]. Analysis of expression patterns also suggests that these transporters are highly regulated and responsive to environmental cues, such as in response to pathogen infection or after wounding.

Additionally, from past studies, the monosaccharide transporter, MST1, was isolated from Nicotiana tabaccum and found to be most strongly expressed in sink tissues including roots, flowers and young leaves [61] where it appears to play a role in unloading of sugars. The protein is homologous to those hexose transport proteins found in Arabidopsis thaliana and Chlorella kessleri and possesses 12 putative membrane-spanning domains which can function as a H^+/monosaccharide symporter just like SUT1, catalyzing the cellular uptake of hexoses (e.g. D-glucose and D-galactose) or pentoses (e.g. D-xylose). Even so, overwhelming evidence from ^{14}C-tracer studies and detailed phloem sap analyses has led to the general consensus in the phloem transport field that sucrose is the predominant sugar substrate that is carried in the sieve tubes of higher plants and transported over long distances to distal tissues [62]. More specifically, hexose sugars do not transport over such long distances.

Furthermore, to the best of our knowledge, no one has seen evidence for the presence of such monosaccharide transporters in the companion cells or sieve tube elements that would facilitate such long-distance transport of hexose sugars. Of course, we cannot deny the fact that our tracer data clearly showed evidence of phloem loading and long-distance transport of ^{18}F-tracer that was derived from ^{18}FDG after its uptake into source leaf-2. This observation is consistent with past observations indicating phloem loading and long distance transport of ^{18}F-tracer after application of ^{18}FDG to sorghum leaf tips [22]. One possible explanation of these observations is that ^{18}FDG is converted to a ^{18}F-sucrose analog that can be actively transported [19]. Alternatively, conversion of ^{18}FDG to its respective sugar alcohol form might provide a mechanism for moving the ^{18}F-tracer. Polyols are reduced forms of aldoses and ketoses, and can be found in all living forms [63]. In some higher plants these sugar alcohols are, together with sucrose, direct products of photosynthesis and serve similar functions as sucrose such as translocation of carbon

skeletons and energy resources between sources and sink organs [64, 65].

Chemical treatments using ISX and MeJA were found to impose interesting systematic differences on the way they affected long-distance transport of ^{18}F-tracer and ^{11}C-photoassimilate that suggests they may act universally on H^+-symport mechanisms. Specifically, ISX was seen to inhibit both phloems reloading of ^{18}F-tracer, as well as long distance transport of ^{11}C-photoassimilate in a dose dependent manner. Classical sugar transport inhibitors like carbonyl cyanide 3-chlorophenylhydrazone (CCCP) behave as protonophores that can shuttle protons across the lipid bilayer of the cell's plasma membrane, and in doing so, uncouple the membrane proton gradient from sugar transport thus shutting down active transport [66]. However, protonophoric activity is not restricted to weakly acidic compounds like CCCP. There are claims that basic compounds like (Z)-5-Methyl-2-[2-(1-naphthyl) ethenyl]-4-piperidinopyridine exhibit protonophoric activity likely due to the amine group [67]. As a weakly basic benzamide, ISX may behave in a similar capacity resulting in its ability to universally shut down sugar transport. Furthermore, we note that past studies have shown that MeJA can re-instate sugar transport after treatment with a classical sugar transport inhibitor like CCCP presumably by re-coupling proton symport. Our observation that MeJA increased long-distance ^{11}C-photoassimilate transport, as well as increased phloem loading and long distance transport of ^{18}F-tracer suggests that its ability to act on the membrane proton gradient serves to increase transport activity of sugars in general.

Our present work also showed that intercellular sugar trafficking was an integral part of the regulatory mechanism for cellulose biosynthesis. Here we used developmental leaf aging as a model for exploring changes in cellulose biosynthesis and for measuring changes in the flux of intra and intercellular sugar resources in the process. Our data clearly demonstrated that ^{18}FDG can be taken up by roots and delivered to all leaf types via xylem transport, and unloaded at the parenchyma symplast-xylem interface where the sugar could migrate from cell-to-cell through the plasmodesmatal cytosolic sleeve in between the plasma membrane and the endoplasmic reticulum. As cells expand and differentiate, their fate determines the extent to which their cytoplasmic connectivity to other cells is maintained [68]. Some cell types, such as those in the leaf mesophyll remain closely connected with their neighboring cells and this connectivity could extend to the parenchyma symplast-xylem interface. However, cytoplasmic continuity is not a constant and will decline with tissue development as simple plasmodesmata (PD) are lost during leaf sink-source transition [69], and the frequency of even the more complex branched PDs decline with maturation [70]. Taken together, we would expect ^{18}FDG's ability to move cell-to-cell via the symplast to systematically decline with aging, consistent with our finding that ^{18}F-tracer flux into ^{18}F-cellulose decreased with increasing leaf age. Furthermore, we were surprised to find that there was no change in the flux of ^{11}C into ^{11}C-cellulose from intracellular sugar sources. What this implies is the cellulose synthetic machinery remained active regardless of leaf age, and that the diminished supply of intercellular sugar was what controlled the process. We tested this hypothesis using ISX and MeJA treatments where from our earlier discussion it was concluded that ISX inhibited sugar transport (both in long-distance movement through the phloem, and in cell-to-cell movement within same tissues) while MeJA enhanced it. Consistent with this model, the inhibition of sugar transport by ISX increased the flux of ^{11}C-tracer into ^{11}C-cellulose from intracellular sugar while it decreased the flux of ^{18}F-tracer into ^{18}F-cellulose from intercellular sugar. Also consistent with this model, the increase in sugar transport by MeJA decreased the flux of ^{11}C-tracer into ^{11}C-cellulose from intracellular sugar while it increased the flux of ^{18}F-tracer into ^{18}F-cellulose from intercellular sugar.

To date, there exists an extensive body of information providing insight into the structural architecture of plant cell walls which are comprised of cellulosic micro fibrils embedded in a matrix of no cellulosic polysaccharides that include heteroxylans and 1,3; 1,4)-β-glucans [71]. Even so, progress in understanding the mechanisms for regulating the synthesis of these macromolecular structures has been relatively slow. For example, past work has shown that β-glucan synthesis, responsible for 1, 3-β-glucan (callose) synthesis in cell wall construction, decreases in activity with plant tissue age [72]. In contrast to this, our work suggests that cellulose synthesis remains uniformly active; at least in developing leaf tissues, and most importantly that intercellular sugar trafficking is a critical component to regulating cell-wall cellulose biosynthesis. We expect that the use of sugar transport mutants could help shed additional light on this highly regulated process and this will certainly be the focus of future studies.

Finally, an area of keen interest is to understand the responses of the plant cell wall to a biotic stresses including drought, flooding, and temperature, or to biotic stresses including attack by pathogens and feeding insects. The effects of these stresses on cell wall metabolism are complex, but important to unravel if we are to build adaptation and/or resistance traits in future cropping systems.

Acknowledgements

This article has been authored by Brookhaven Science Associates, LLC under contract number DE-SC0012704 with the U.S. Department of Energy, Office of Biological and Environmental Research. Additional support was provided by the German Academic Exchange Service (Deutscher Akademischer Austauschdienst, DAAD) Bonn. The United States Government retains and the publisher, by accepting the article for publication, acknowledges that the United States Government retains a non-exclusive, paid-up, irrevocable, world-wide license to publish or reproduce the published form of this manuscript, or allow others to do so, for United States Government purposes. The authors would like to acknowledge B. Rooney for his assistance in acquiring the MR image, D. Alex off and C. Shea for their assistance in preparing ^{18}FDG, and D. Braun for providing feedback during manuscript preparation.

References

1. Saxena IM, Brown RM. Cellulose biosynthesis: current views and evolving concepts. *Annals of Botany.* 2005;96(1):9–21.
2. Carpita NC, Ralph J, McCann MC. "The Cell Wall," in Biochemistry & Molecular Biology of Plants, 2nd ed. (eds. Buchanan B.B., Gruissem W., Jones R.L.) Published 2015 by John Wiley & Sons, Ltd. Chapter 2, pp 45-110.
3. Huggenberger F, Jennings EA, Ryan PJ, Burrow KW. (1982) Isoxaben, a new selective herbicide for use in cereals. *Weeds* **1**, 47-52.
4. Amiard V, Demmig-Adams B, Mueh KE, Turgeon R, Combs AF, Adams WW III. Role of light and jasmonic acid signaling in regulating foliar phloem cell wall in growth development. *New Phytol.* 2007;173(4):722–731.
5. Hanik N, Gómez S, Best M, Schueller MJ, Orians CM, Ferrieri RA. Partitioning of new carbon as ^{11}C in *Nicotiana tabacum* reveals new insight into methyl jasmonate induced changes in metabolism. *J. Chem. Ecol.* 2010;36(10):1058-1067.
6. Hanik N, Gómez S, Schueller MJ, Orians CM, Ferrieri RA. Use of gaseous 13NH3 administered to intact leaves of *Nicotiana tabacum* to study changes in nitrogen utilization during defense induction, *Plant Cell & Environ*. 2010;33(12):2173-2179.
7. Caño-Delgado A, Penfield S, Smith C, Catley M and Bevan M. Reduced cellulose synthesis invokes lignification and defense responses in *Arabidopsis thaliana*. *Plant Journal*. 2003;34(3):351–362.
8. Ellis C, Turner JG. The *Arabidopsis* mutant *cev1* has constitutively active jasmonate and ethylene signal pathways and enhanced resistance to pathogens. Plant Cell. 2001;13(5):1025–1033.
9. Carpita NC, Gibeaut DM. Structural models of primary cell walls in flowering plants: consistency of molecular structure with the physical properties of the walls during growth. *Plant J.* 1993;3(1):1–30.
10. Somerville C, Bauer S, Brininstool G, Facette M, Hamann T and Milne J, et al. Toward a systems approach to understanding plant cell walls. *Science.* 2004;306:2206–2211.
11. Somerville C. Cellulose synthesis in higher plants. *Annu. Rev. Cell Dev. Biol.* 2006;22:53–78.
12. Fujimoto M, Ueda T. Conserved and plant-unique mechanisms regulating plant post-Golgi traffic. *Front Plant Sci.* 2012;3:197.
13. Ebine K, Ueda T. Roles of membrane trafficking in plant cell wall dynamics. *Frontiers in Plant Sci.* 2015;6:878.
14. McFarlane HE, Watanabe Y, Yang W, Huang Y, Ohlrogge J, Samuels AL. Golgi- and trans-golgi network mediated vesicle trafficking is required for wax secretion from epidermal cells. *Plant Physiol.* 2014;164(3):1250–1260.
15. Kim SJ, Brandizzi F. The plant secretory pathway: an essential factory for building the plant cell wall. *Plant Cell Physiol.* 2014;55(4):687–693.
16. Fujimoto M, Tsutsumi N. Dynamin-related proteins in plant post-Golgi traffic. *Front Plant Sci.* 2014;5:408.
17. Best M, Kaitlyn Koenig K, McDonald K, Schueller MJ, Rogers A and Ferrieri RA. Inhibition of trehalose breakdown increases new carbon partitioning into cellulosic biomass in *Nicotiana tabacum. Carbohydrate Res.* 2011;346(5):595–601.
18. Oechel WC, Lawrence W. "Carbon allocation and utilization," in Ecological Studies (vol.39), Resource use by Chaparral and Matorral: A Comparison of Vegetative Function in Two Mediterranean Type Ecosystems (ed. P.C. Miller), pp. 224-226, Springer-Verlag, New York, 1981.
19. Rotsch D, Brossard T, Bihmidine S, Ying W, Gaddam V and Harmata M, et al. Radiosynthesis of 6'-deoxy-6'[^{18}F]fluorosucrose via automated synthesis and its utility to study *in vivo* sucrose transport in maize (*Zea mays*) leaves. PLoS ONE. 2015;10(5):e0128989.
20. Leach KA, Tran TM, Slewinski TL, Meeley RB, Braun DB. Sucrose transporter2 contributes to maize growth, development, and crop yield. *J. Integr Plant Biol.* 2017;59(6):390-408.
21. Tsuji AUH, Yamashita T, Matsuhashi S, Ito T, Mizuniwa C and Ishioka NS, et al. Uptake of ^{18}FDG and 13NO3- in tomato plants, in *TIARA Annual Report 2001*, Vol.35, (eds. Saidoh M, Toraishi A, Namba H, Itoh H, Tanaka S, Naramoto H.) Japan Atomic Energy Research Institute, Ibaraki, Japan, 2002;103–104.
22. Hattori E, Uchida H, Harada N, Ohta M, Tsukada H and Hara Y, et al. Incorporation and translocation of 2-deoxy-2-[^{18}F]fluoro- D-glucose in Sorghum bicolor (L.) Moench monitored using a planar positron imaging system. *Planta*. 2008;227(5):1181–1186.
23. Li S, Liu L, Jiang H, Zhang J, Pan P, Zhang S, Guo J, Zhang J, Yang J. It was found that amino sugar nitrogen was a source of energy for plant. *J. Agric Sci.* 2014;6(2):45-53.
24. Partelová D, Uhrovčík J, Lesný J, Horník M, Rajec P, Kováč P, Hostin S. Application of positron emission tomography and 2-[^{18}F]fluoro-2-deoxy-D- glucose for visualization and quantification of solute transport in plant tissues. *Chem. Pap.* 2014;68:1463–1473.
25. Meldau S, Woldemariam MG, Fatangare A, Svatos A, Galis I. Using 2-deoxy-2-[^{18}F]fluoro-D-glucose ([^{18}F]FDG) to study carbon allocation in plants after herbivore attack. *BMC Res.* 2015;8:45
26. Fatangare A, Svatoš A. Application of 2-deoxy-2-fluoro-D-glucose (FDG) in plant imaging: Past, present and future. *Front. Plant Sci.* 2016;7:483.
27. Ferrieri AP, Appel H, Ferrieri RA, Schultz JC. Novel application of 2-[^{18}F] fluoro-2-deoxy-D-glucose to study plant defenses. *Nucl Med Biol.* 2012;39(8):1152-1160.
28. Huggenberger F, Jennings EA, Ryan PJ, Burrow KW. (1982) Isoxaben, a new selective herbicide for use in cereals. *Weeds* **1**, 47-52.
29. Hattori E, Uchida H, Harada N, Ohta M, Tsukada H and Hara Y, et al. Incorporation and translocation of 2-deoxy-2-[^{18}F]fluoro- D-glucose in Sorghum bicolor (L.) Moench monitored using a planar positron imaging system. *Planta*. 2008;227(5):1181–1186.
30. Montezinos D, Delmer DP. Characterization of inhibitors of cellulose synthesis in cotton fibers. *Planta.* 1980;148(4):305-311.
31. Heim DR, Roberts JL, Pike PD, Larrinua IM. A second locus, Ixr B1 in *Arabidopsis thaliana*, that confers resistance to the herbicide isoxaben. *Plant Physiol.* 1990;92(3):858-861.
32. Peng L, Kawagoe Y, Hogan P, Delmer D. Sitosterol-beta-glucoside as primer for cellulose synthesis in plants. *Sci.* 2002;295:147-150.
33. Wasternack C. Jasmonates: an update on biosynthesis, signal transduction and action in plant stress response, growth and development. *Annals of Bot.* 2007;100(4):681–697.

34. Ferrieri AP, Agtuca B, Appel H, Ferrieri RA, Schultz JC. Getting to the root of the problem: methyl jasmonate induces temporal changes in carbon transport and partitioning in *Arabidopsis thaliana* that depend on root-shoot signaling, *Plant Physiol*. 2013;161(2):692-704.
35. Ferrieri RA, Wolf AP. The chemistry of positron emitting nucleogenic (hot) atoms with regard to the preparation of labeled compounds of practical utility. *Radiochim Acta*. 1983;34**:**69– 83.
36. Ferrieri RA, Gray DW, Babst BA, Schueller MJ, Schlyer DJ and Thorpe MR, et al. Use of carbon-11 in Populus shows that exogenous jasmonic acid increases biosynthesis of isoprene from recently fixed carbon, *Plant, Cell & Environment.* 2005;28(5)591-602.
37. Kume T, Matsuhashi S, Shimazu M, Ito H, Fujimura T and Adachi K, et al. Uptake and transport of positron-emitting tracer (^{18}F) in plants. *Appl Radiat Isot*. 1997;48(8):1035–1043.
38. Nakanishi TM, Yokota H, Tanoi K, Ikeue N, Okuni Y and Furukawa J, et al. Comparison of 15O-labeled and ^{18}F-labeled water uptake in a soybean plant by PETIS (Positron Emitting Tracer Imaging System). *Radioisotopes.* 2001;50:265–269.
39. Nakanishi TM, Tanoi K, Yokota H, Kang D.-J, Ishii R and Ishioka NS, et al. ^{18}F used as tracer to study water uptake and transport imaging of a cowpea plant. *J. Radioanal. Nucl. Che*m. 2001;249(2):503–507.
40. Wasternack C. Jasmonates: an update on biosynthesis, signal transduction and action in plant stress response, growth and development. *Annals of Bot.* 2007;100(4):681–697.
41. Maschauer S, Prante O, Hoffmann M, Deichen JT, Kuwert T. Characterization of ^{18}F-FDG uptake in human endothelial cell *in vitro. J. Nucl. Med*. 2004;45(3):455-460.
42. Heiniger U, Delmer DP. UDP-glucose: Glucan synthetase in developing cotton fibers: II. Structure of the reaction product. *Plant Physiol*. 1977;59:719–723.
43. Maltby D, Carpita NC, Montezinos D, Kulow C, Delmer DP. β-1,3-Glucan in Developing Cotton Fibers. *Plant Physiol.* 1979;63(6):1158–1164.
44. Dugger WM, Palmer RL. Effect of boron on the incorporation of glucose from UDP-595 glucose into cotton fibers grown *in vitro. Plant Physiol*. 1980;65:266–273.
45. Zhong H, Läuchli A. Incorporation of [14C] glucose into cell wall polysaccharides of cotton roots: Effects of NaCl and CaCl2. *Plant Physiol.* 1988;88(3):511–514.
46. Dubois M, Gilles KA, Hamilton JK, Roberts PA and Smith F. Colorimetric method for determination of sugars and related substances. *Anal. Chem*. 1956;28(3):350–356.
47. Rennie EA, Turgeon R. A comprehensive picture of phloem loading strategies. *Proc. Natl. Acad. Sci*, USA. 2009;106(33):14162-14167.
48. Slewinski TL, Braun DM. Current perspectives on the regulation of whole-plant carbohydrate partitioning. *Plant Sci.* 2010;178(4):341–349.
49. Sauer N. Molecular physiology of higher plant sucrose transporters. *FEBS Lett*. 2007; 581(12):2309-2317.
50. Braun DM, Wang L, Ruan YL. Understanding and manipulating sucrose phloem loading, unloading, metabolism, and signalling to enhance crop yield and food security. *J Exp. Bot.* 2014;65(7):1713-1735.
51. Bürkle L, Hibberd JM, Quick WP, Kühn C, Hirner B and Frommer WB. The H+-sucrose cotransporter NtSUT1 is essential for sugar export from tobacco leaves. *Plant Physiol*. 1998;118(1):59-68.
52. Chen L.-Q, Cheung LS, Liang Feng L, Tanner W and Frommer WB. Transport of Sugars. *Annu Rev Biochem*. 2015;84:865–894.
53. Sauer N, Tanner W. The hexose carrier from *Chlorella.* cDNA cloning of a eucaryotic H+-cotransporter. *FEBS Lett*. 1989;259(1):43–46.
54. Maynard JW, Lucas WJ. Sucrose and glucose uptake in *Beta vulgaris* leaf tissue. A case for a general (apoplastic) retrieval system. *Plant Physiol*. 1982;70(5):1436–1443.
55. Getz HP, Knauer D, Willenbrink J. Transport of sugars across the plasma membrane of beetroot protoplasts. *Planta.* 1987;171(2):185–196.
56. Gogarten JP, Bentrup FW. (1989) Substrate specificity of the hexose carrier in the plasma membrane of *Chenopodium* suspension cells probes by transmembrane exchange diffusion. *Planta* 178, 52–60.
57. Tubbe A, Buckhout TJ. *In vitro* analysis of the H1-hexose symporter on the plasma membrane of sugarbeets (*Beta vulgaris* L.). *Plant Physiol*. 1995;99:945–951.
58. Sauer N, Friedländer K, Gräml-Wicke U. Primary structure, genomic organization and heterologous expression of a glucose transporter from *A. thaliana. EMBO J.* 1990;9(10):3045–3050.
59. Büttner M, Sauer N. Monosaccharide transporters in plants: structure, function and physiology. *Biochim Biophys Acta.* 2000;1465(1-2):263–274.
60. Truernit E, Schmid J, Epple P, Illig J, Sauer N. The sink-specific and stress-regulated *Arabidopsis* STP4 gene: Enhanced expression of a gene encoding a monosaccharide transporter by wounding, elicitors, and pathogen challenge. *Plant Cell.* 1996; 8(12):2169–2182.
61. Sauer N, Stadler R. A sink-specific H+/monosaccharide co-transporter from *Nicotiana tabacum*: cloning and heterologous expression in baker's yeast. *The Plant Journal. 1993;* 4(4):601-610.
62. Liu DD, Chao WM, Turgeon R. Transport of sucrose, not hexose, in the phloem. *J.Exp. Bot*. 2012;63(11):4315–4320.
63. Noiraud N, Maurousset L, Lemoine R. Identification of a mannitol transporter, AgMaT1, in celery phloem. *Plant Cell*. 2001;13(3);695–705.
64. Noiraud N, Maurousset L, Lemoine R. Transport of polyols in higher plants. *Plant Physiol. Biochem*. 2001;39(9):717–728.
65. Conde A, Silva P, Agasse A, Conde C, Geró H. Mannitol transport and mannitol dehydrogenase activities are coordinated in *Olea europaea* under salt and osmotic stresses. *Plant Cell Physiol*. 2011;52(10):1766–1775.
66. Thorpe MR, Ferrieri AP, Herth MM, Ferrieri RA. Imaging transport of methyl jasmonate and photoassimilate: jasmonate moves in both phloem and xylem and restores sugar transport after proton transport is decoupled. *Planta*. 2007;226(2):541-551.
67. Schwaller MA, Allard B, Lescot E, Moreaui F. Protonophoric activity of ellipticine and isomers across the energy-transducing memebrane of mitochondria. *J. Biol. Chem*. 1995;270:22709-22713.
68. Mezitt LA, Lucas WJ. Plasmodesmal cell-to-cell transport of proteins and nucleic acids. *Plant Molecular Biology*. 1996;32(1-2):251-273.

69. Roberts IM, Boevink P, Roberts AG, Sauer N, Reichel C and Oparka KJ. Dynamic changes in the frequency and architecture of plasmodesmata during the sink-source transition in tobacco leaves. *Protoplasma*. 2001;218(1-2):31-44.
70. Roberts AG, Oparka KJ. Plasmodesmata and the control of symplastic transport. *Plant, Cell and Environment.* 2003;26(1):103-124.
71. Dimitroff G, Little A, Lahnstein J, Schwerdt JG, Srivastava V and Bulone V, et al. (1,3; 1,4)-β-Glucan biosynthesis by the CSLF6 enzyme: position and flexibility of catalytic residues influences product fine structure. *Biochem*. 2016;55(13):2054-2061.
72. Dugger WM, Palmer RL, Black CC. Changes in β-1,3-glucan synthase activity in developing lima bean plants. *Plant Physiol*. 1991;97(2):569-573.